ON THE SPATIO-TEMPORAL STRUCTURE OF THE CYLINDER WAKE

I. Peschard[①], P. Le Gal[①] and Y.Takeda[②]

[①]Institut de Recherche sur les Phénomènes Hors Equilibre

UM 138, CNRS - Universités d'Aix-Marseille I & II

12, Avenue Général Leclerc,13003 Marseille, France

[②]Laboratory for Spallation Neutron Source

Paul Scherrer Institute

CH-5232 Villigen PSI, Switzerland

ABSTRACT

The wake of a short aspect ratio cylinder placed in a uniform flow is experimentally investigated. After having characterized the temporal behavior of the Bénard-Von Kàrmàn vortex shedding by the use of a classical hot-wire anemometer, an ultrasound anemometry technique is applied to study the spatial critical behavior of the envelope of the transversal velocity of the wake. It is shown that this envelope which represents the spatial form of the global mode of the wake, follows universal scaling lawswhich are in agreement with a second order phase transition. In a second set of experiments, the behavior of the longitudinal velocity fluctuations is also investigated. It has also been discovered that there is a special point several diameters behind the cylinder, which plays a role of a wave maker. Finally, for very small aspect ratio cylinders, symmetric vortex shedding is reported and modeled using a system of coupled oscillators equations.

List of symbols

Symbol	Unit	Physical Property
A	mm/s or a.u	amplitude of velocity oscillation.
A_{max}	mm/s	maximum of amplitude of velocity oscillation
c_2	-	non linear parameter of Landau equation
d	mm	diameter of cylinder
l	mm	length of cylinder
$\Gamma=l/d$	-	aspect ratio of cylinders
x	mm	longitudinal downstream coordinate
y	mm	transversal coordinate
x/d	-	normalized longitudinal downstream coordinate
y/d	-	normalized transversal coordinate
x_{max}	mm	reduced position of the maximum of amplitude
R	-	Reynolds number
R_c	-	critical Reynolds number
ε	-	reduced Reynolds number $(R-R_c)/R_c$
δ	mm	typical viscous length
ω_0	-	natural frequency of the shedding

1

Introduction

The goal of this study is to analyse the temporal and the spatial features of the classical Bénard-Von Kàrmàn wake of a cylinder. Although this wake is certainly the most popular flow in fluid mechanics, many problems about its spatio-temporal structure remain open. Recently, it has been proved by several authors (Sreenivasan et al (1986), Provansal et al (1987), Dusek et al (1994) and Schumm et al (1994)) that the Bénard-Von Kàrmàn vortex street shed by a cylinder, appears via a Hopf bifurcation at a critical Reynolds number R_c. When neglecting the three-dimensional features of the wakes, the normal form for this bifurcation is called the Landau equation and reads simply:

$$\frac{dA}{dt} = (\varepsilon + i \omega_0) A - (1 + i c_2) |A|^2 A \qquad (1)$$

where A is a complex order parameter representing the lateral velocity measured at one location in the wake, ε the reduced Reynolds number $((R - R_c)/R_c)$, ω_0 the natural frequency (without the non linear correction) of the shedding at Reynolds number R and c_2 a parameter corresponding to this frequency variation with the finite amplitude oscillations of the velocity field. The universal value for c_2 is equal to -2.7 (see for instance Dusek et al (1994)) for infinitely long circular cylinder. In fact, Albarède and Monkewitz (1992) have shown that this model of two-dimensionnal wake can be extended to the case of the three-dimensionnal wake, and in particular in order to interpret the "chevron shedding" observed by Williamson (1989). Moreover, it has also been shown by Albarède and Provansal (1995), that when the aspect ratio of the cylinder is small enough, only the first mode (along the axis of the cylinder) of vortex shedding can be observed. In these conditions, the temporal behavior of the wake is accurately described by the Landau equation. Of course, the coefficients of the model have to be estimated again as they depend on the aspect ratio of the cylinder. In particular, it is known from Lee and Budwig (1990) that the critical Reynolds number increases when the aspect ratio of the cylinder is decreased. Although these substantial progress achieved by these theoretical and experimental investigations concerning the temporal behavior of the wake,

Goujon-Durand et al (1994) and later, Zielinska and Wesfreid (1995) and Wesfreid et al. (1996) stressed on the signification of the amplitude A of the global mode. They showed experimentally and numerically that A has to be a norm of the spatial amplitude distribution of the wake which is different from a local amplitude as it was usually considered in experiments. Analysing the deformation of the spatial envelope of the wake oscillations with the Reynolds number , they were able to prove by hot wire mappings of the flow or direct numerical simulation of the wake, that the position x_{max} (on the downstream direction) of the maximum A_{max} of the velocity oscillation, approaches the cylinder as the Reynolds number increases. Moreover, they showed that A_{max} obeys the Landau equation and that x_{max} varies with a power law of the Reynolds number. These results are in complete agreement with the prediction from a second order phase transition.

The present experimental investigation, which is based on a new and particularly well-adapted anemometer, namely an ultrasound velocity profiler, brings a verification of this critical behavior of the wake near its threshold. Then, motivated by some of these measurements, we present some original visualizations of a varicose instability of the wake behind a very small aspect ratio cylinder.

2

Experimental arrangement and techniques

Our experimental facility consists of a water loop and is fully described by Le Gal et al (1996). The test section is 20 mm high and 128 mm wide. The water velocity can be varied between 0 and 1 m/s. It is measured by a home-made flow-meter and the back-ground turbulence intensity of the flow has been estimated by a hot-wire anemometer as about 0.5 %. To avoid the emergence of three-dimensionnal shedding, a small aspect ratio cylinder having a diameter d equal to 4 mm, is positionned on one of the horizontal walls of the channel. Its length is l=20 mm (l/d=5) and it is in close contact with the other horizontal wall. As the cylinder touches the opposite wall and because no end-plates have been used to control the boundary conditions, horse-shoe vortices are created in the boundary layers of the walls of the

water tunnel, around the ends of the cylinders. However, it is observed by visualisations and by ultrasound measurements that the alternate vortex shedding in the bulk flow is only slightly affected by the presence of these vortices. In the first part of this study, a classical hot-wire study of the temporal behavior of the wake is performed with a pobe placed seven diameter downstream the cylinder (x/d=7, y/d=0). The parameters of the Landau equation are calculated by a classical procedure based in particular on the impulse response of the wake. Then, its spatial shape is studied by ultrasound anemometry whose operation principle is ultrasound echography. An ultrasonic 4 MHz frequency pulse is emitted through the water flow by a piezoelectric probe having a diameter of 8 mm. The sound beam (roughly 5mm in diameter) propagates inside the flow and is reflected by 100 microns hydrogen bubbles which are generated by a electrolysis of water using a 0,1 mm platinium wire stretched across and at midheight of the channel, 100 mm upstream of the cylinder. When the piezoelectric transducer recieves the echoes back, the anemometer calculates the position of the reflecting bubbles by the time delay between the emitted and the recieved pulse, as well as the Doppler shift they generate because of their own velocity. More details about this technique can be found in Takeda et al (1993). When correctely seeded, the flow can be analysed by the measurements of instantaneous velocity profiles projected onto the direction of the sound beam. We performed to two sets of experiments. In the first, the ultrasound probe is placed in a groove machined in the middle plane of the side-wall of the channel. By this configuration, the transversal velocity profiles can be measured along lines crossing the main flow in the y direction. The transversal velocity profiles are recorded every 69.8 ms (or for some experiments, every 135.3 ms), in 128 spatial positions separated by 0.74 mm. 1024 instantaneous profiles are then recorded for several Reynolds numbers R. In the second set of experiments, the ultrasound probe is positionned inside the water flow, 80 mm downstream of the cylinder (x/d= 20) and 2 mm on its side (y/d= 0.5) in such a manner that longitudinal velocity profiles can be recorded.

3

Hot-wire determination of the temporal features of the wake

In the experimental conditions described in section 2, the critical Reynolds number R_c is determined by a careful hot-wire study of the wake. In particular, when studying the impulse response of the wake at different Reynolds numbers, the shedding frequency and the decay rate of the oscillations are obtained under the threshold. This study is then completed above the threshold, where the amplitude and the frequency of the saturated regimes are measured. The critical value (R_c=102±2) that we obtain agrees perfectly well with the previous study of Lee and Budwig (1990) concerning small aspect ratio cylinder wakes. The determination of the coefficient c_2 leads to a value equal to -1±0.1 which completes the study of Albarède and Provansal (1995). Figure 1 shows the evolution of the frequency (a) and of the square of the amplitude (b) of the wake, measured on the axis, at 7 diameters downstream the cylinder. The change of slope of the frequency curve is reminiscent of the non linear feature of the wake oscillation and the ratio between the two slopes leads to the deternination of the c_2 coefficient. Note also on Figure 1-b, that the prediction of the Landau equation - i.e. that the amplitude of the saturated oscillations above the threshold has to be proportionnal to the square root of the threshold distance- seems to be valid only for Reynolds numbers less than 160. Above this value, we note a saturation of the square of the amplitude that deviates from the linear prediction. Next section which presents a global description of the wake will give an explanation of this saturation.

4

Ultrasound measurements of the spatial shape of the global mode

Modelling the Bénard-Von Kàrmàn instability in terms of global modes, needs to represent the velocity wake fluctuations by the product of two independent functions linked to the

temporal and to the spatial evolutions of the velocity field. As we saw in the previous section, the main temporal features of the wake can be described by local measurements of the velocity flow. On the contrary, the spatial behavior of the periodic disturbances is much more difficult to study because traditionnal anemometry techniques (hot wire or laser anemometry) need heavy mappings of the flow. The ultrasound profile monitor presents in this context a new and interesting alternative.

4.1

Transversal velocity profiles

The early experimental studies of Mathis (1983) showed already that the envelope of the fluctuations of the wake possesses a maximum whose position varies with the Reynolds number. More recently, the experimental work of Goujon-Durand et al (1994) and Wesfreid et al. (1996) and the numerical investigations of Zielinska and Wesfreid (1995) have shown that the wakes of triangular bodies present a critical behavior at Reynolds numbers close to the instability threshold. In particular, it is shown that the amplitude and the position of the maxima of the transversal velocity oscillations obey power laws of the Reynolds number.

Using the ultrasound profiler, we measured the complete profiles of the transversal velocity at 8 different longitudinal positions downstream the cylinder and for several Reynolds numbers. Figure 2-a presents such a space-time diagram recorded at a Reynolds number of 132 at the position x/d = 6. The 2-D Fourier Transform of this space-time diagram is then calculated and band-pass filtered, in order to improve the visualisation of the vortex shedding (see Figure 2-b). The gray level coding permits to observe the periodic oscillation of the transversal velocity due to the vortex shedding. As shown by Dusek (1996), the transversal velocity mode is symmetric versus the flow axis as it can be seen by our measurements. This corresponds to the classical alternate vortex shedding or to the sinuous mode of the wake. Then, taking the temporal Fourier Transform for each of the 128 space points, it is possible to compute the spatial distribution of the squared amplitude of the

fundamental mode at those longitudinal positions. These profiles are then displayed on the same diagram giving a three-dimensionnal view of the global mode of the circular cylinder wake. Figure 3 shows these spatial shapes of the wake as the Reynolds number increases. It can be observed that the energy profiles of the first x-location profiles has a double hump near the cylinder. Further downstream, these profiles are transformed into a single peak. We will come back later on this double hump structure, and analyse for now the evolution of the main peak. Plotting the amplitudes taken by these profiles at y=0, we show on Figure 4 the deformation of the global mode with the Reynolds number. The deformation which can be easily observed, is at the origin of the amplitude saturation displayed on Figure 1-b. We observe a rapid increase of the amplitude of oscillation from zero near the cylinder, up to a maximum A_{max} whose position x_{max} varies between 9 and 5, when increasing the Reynolds number. Then, the decrease of these envelopes far away from the cylinder can be interpreted as a viscous relaxation of the far wake.

It is then easy to compute the evolution of the position and level of the maximum of the mode as a function of the Reynolds number. The logarithmic representations of figure 5-a and 5-b show the critical behavior of the envelops as already observed by Goujon-Durand et al (1994), Zielinska and Wesfreid (1995) and Wesfreid et al.(1996). Moreover, we confirm the exponent of the power laws (1/2 for the amplitude A_{max} and -1/2 for the position x_{max}) observed by these authors. Note that these exponents are in complete agreement with a second-order phase transition model of the wake. An improvement of the Landau model can be acchieved when adding to equation (1) a second-derivative-term in the x direction. In order to enhance the scale-invariance structure of the wake, we renormalize the amplitude and the space by using A_{max} and x_{max}. Figure 6 shows that the different envelopes now collapse onto a single curve.

As already mentioned, very near the cylinder (x/d between 1 and 4), the energy of the global mode presents a double hump structure (see Figure 3). In fact, they correspond to measurements which were realised at longitudinal positions inside the recirculation eddies formed behind the cylinder. Therefore, the double hump structure corresponds to a wave propagation on each side of the cylinder. We show such a space-time measurement for R=120

and x/d=2, in Figure 7-a). As in Figure 2, we use the Fourier Transform and a band-pass filter to enhance the wake structure (Figure 7-b). It can be observed that the oscillations on each side of the cylinder, are in phase, but for some Reynolds numbers, it has also been possible to observe for some periods of time, oscillations in phase opposition. In this case, the shedding is a mixture of a symmetric and anti-symmetric oscillations. Figure 8 shows for a Reynolds number of R=150 and a longitudinal abscissa x/d=3, such a case of mixing between the varicose (anti-symmetric transversal velocity fluctuations) and the sinuous (symmetric transversal velocity fluctuations) mode. We will confirm further the presence of the varicose mode of vortex shedding in section 5, where a visual study of very short aspect ratio cylinders is presented.

4.2

Longitudinal velocity profiles

The ultrasound probe is now placed inside the water channel, aligned with the x axis in order to measure the longitudinal velocity fluctuations from the longitudinal location x/d=20 up to the cylinder. Because this mode is odd, its amplitude is null along the x axis, and we placed the probe at the transversal position y/d= 0.5. Figure 9-a and 9-b give space-time diagrams obtained by the ultrasound profiler. As it can be clearly observed on these figures, two systems of waves which are generated from a position around x/d=3.5 downstream of the cylinder. The waves propagating in the downstream direction between x/d=3.5 and 20 correspond to the alternate shedding of the travelling vortices. The other waves propagate to the upstream direction between x/d=3.5 and the cylinder on the edge of the stationnary recirculating eddies. These experimental observations of the cylinder wake, may confirm the theoretical predictions of the existence of a region of the flow where the instability is of "absolute type" as it is defined in the review of Huerre and Monkewitz (1990).

5

Visualization of very short aspect ratio cylinder wakes

To verify the presence of the varicose mode of vortex shedding, we placed in the water channel, cylinders having aspect ratios Γ as small as 0.5. The wake is visualized by injecting (at an appropriate very small rate) white dye by small holes placed at the middle of the transversal plane, at the rear face of the cylinder. Figure 10 presents a sequence of snapshots obtained at different Reynolds numbers. As predicted by Lee and Budwig (1990), the threshold of the vortex shedding is pushed toward high Reynolds numbers. Moreover, as it can be seen on figure 10, the first instability of the wake in such conditions is of varicose type. For this particular cylinder, this instability occurs for a Reynolds number around 440. Although the main features of the flow are two-dimensional, we believe that it is the three-dimensional structure (and not shedding) of the near wake which is at the origin of this varicose mode. Under this threshold, the wake remains stationary with the formation of large recirculating eddies behind the cylinder (see Figure 10-a). Above the threshold, a symmetric oscillation develops on each side of the recirculating eddies (Figure 10-b-c). We note also on these snapshots the existence next to the cylinder of a dead water zone which traps the dye. The extension of this region is approximatively one half of a diameter. When increasing the Reynolds number, the varicose mode generates a symmetric vortex street. Finally for R=800 (Figure 10-e), the classical alternate shedding appears. First both modes exist together, but for R=900 (see Figure 10-f) the alternate shedding and its associated Bénard-Von Kàrmàn vortex street dominate the wake. A physical interpretation of this phenomenon can be proposed if we consider the oscillating wake as the result of the coupling between two shear layers which have a thickness given by viscous effects and which are located on each side of the cylinder. Following the work we made on two coupled wakes (see Peschard and Le Gal (1996)), we propose to model these two unstable shear layers by two linearly coupled Hopf bifurcations of the type described by equation (1). As it was demonstrated for two wakes, the in-phase mode appears for strongly coupled oscillators and the phase-opposition mode appears for weakly coupled wakes. We can therefore extrapolate these observations to the case of a single wake. The two shear layers have a thickness approximately

given by the viscous scale of the flow: $\delta=\nu/U$ where ν is the kinematic viscosity of the fluid and U its velocity. It is then easily shown that the ratio between the distance separating the shear layers and their thickness is $d/\delta= R$. Therefore, near the threshold of very small aspect ratio cylinders ($R_c\cong500$), this ratio which gives the coupling strengh between the oscillators, is large and our model predicts a phase-opposition locking which gives a varicose mode of vortex shedding. On the contrary, large aspect ratio cylinders have relatively close shear layers: $d/\delta \cong50$ and then are strongly coupled. The sinuous mode appears in this case. Note that a similar oscillators model based on coupled Van der Pol oscillators has been recently proposed by Lopez-Ruiz and Pomeau (1996). They obtained similar results to ours (Peschard and Le Gal (1996)) to interpret the transition between a varicose and a sinuous mode of vortex shedding phenomena. Note also that a similar mode selection (see for instance Thomas and Prakash (1990)) works generally for two-dimensional jets: undeveloped "flat" profiles jets are unstable to the varicose mode (weakly coupled shear layers) contrary to well developed parabolic profile jets (strongly coupled shear layers) which are unstable to the sinuous mode.

6
Conclusion

The present experimental study of small aspect ratio cylinder wakes has confirmed and revealed new phenomena occuring on the vortex shedding. First, a classical hot wire anemometry study showed that even small aspect ratio ($\Gamma=l/d=5$) cylinder wakes still appear via Hopf bifurcations. The parameters of the bifurcation agree fairly well with the existing linear or non linear data. Following Westfreid and co-workers, it was also proved that the spatial shape of the global mode of the wake obeys universal phase transition laws. This last study was realized by the use of an ultrasound anemometer that permits to avoid extended mapping of the flow. Transversal and longitudinal velocity profile measurements have been successfully performed. At 3.5 diameters downstream the cylinder, we observe the existence of a special location from where waves are emitted in the downstream and upstream

directions. This may be the signature of the so-called absolute instability of the wake. The ultrasound measurements revealed also the presence of a symmetric vortex shedding. The presence of this varicose mode has then been checked by flow visualisation on a very small aspect ratio cylinder (l/d=0.5). An interpretation in terms of coupled oscillators was finally presented where the aspect ratio of the cylinders drives the coupling between the shear layers which develop on each side of the cylinders.

References

-**Albarede P; Monkewitz P** (1992) A model for the formation of oblique shedding and "chevron" patterns in cylinder wakes, Phys. Fluids A 4: 744-756.

-**Albarède P; Provansal M** (1995) Quasi-periodic cylinder wakes and the Ginzburg-Landau model, J. Fluid Mech. 291: 191.

-**Dusek J** (1996) Spatial structure of the Bénard-Von Kàrmàn instability, Eur; J; Mech. B/Fluids 15 (3): 330.

-**Dusek J; Le Gal P; Fraunié Ph** (1994) A numerical and theoretical study of the first Hopf bifurcation in a cylinder wake, J. Fluid Mech. 264: 59-80.

-**Goujon-Durand S; Wesfreid JE; Jenffer P (1994)** Downstream evolution of the Bénard-Von Kàrmàn instability, Phys. Rev. E 50: 308.

-**Huerre P; Monkewitz P (1990)** Local and global instabilities in spatially developing flows, Annu. Rev. Fluid Mech. 22: 473.

-**Lee T; Budwig R** (1990) A study of the effect of aspect ratio on vortex shedding behind circular cylinders, Phys. Fluids A 3 (2): 309-314.

-**Lopez-Ruiz R; Pomeau Y** (1996) Non linear transition between two oscillation modes. (A model for the release of vortices behind a circular cylinder), submitted to Phys. Rev. E.

-**Mathis C** (1983) Propriétés des composantes transverses dans l'écoulement de Bénard-Von Kàrmàn aux faibles nombres de Reynolds. Thèse de l' Univ. de Provence, France.

-**Peschard I; Le Gal P** (1996) Coupled wakes of cylinders, Phys. Rev. Lett. 77 (15):3122-3125.

-**Provansal M; Mathis C; Boyer L** (1987) Bénard-von Karman instability: transient and forced regimes, J. Fluid Mech. 182: 1-22.

-**Sreenivasan KR; Strykowski PJ; Olinger DJ** (1986) Hopf bifurcation, Landau equation and vortex shedding behind circular cylinders, Proc. Forum on Unsteady Forum Separation (ed. K. N. Ghia), ASME FED, 52: 1-13.

-**Schumm M; Berger E; Monkewitz P** (1994) Self-excited oscillations in the wake of two-dimensional bluff bodies and their control, J. Fluid Mech. 271: 17-53.

-**Takeda Y; Fischer WE; Sakakibara J; Ohmura K** (1993) Experimental observation of the quasi periodic modes in a rotating Couette system, Phys. Rev. E 47: 4130.

-**Thomas FO; Prakash KMK** (1991) An experimental investigation of the natural transition of an untuned planar jet. Physics of Fluids A 3 (1): 90-105.

-**Wesfreid JE; Goujon-Durand S; Zielinska BJA** (1996) Global mode behavior of the streamwise velocity in wakes, J. Phys. II, France, 6 : 1343-1357

-**Williamson CHK** (1989) Oblique and parallel modes of vortex shedding in the wake of a circular cylinder at low Reynolds numbers, J. Fluid Mech. 206: 579-627.

-**Zielinska BJA; Wesfreid JE** (1995) On the spatial structure of global modes in wake flow, Phys. Fluids 7: 6.

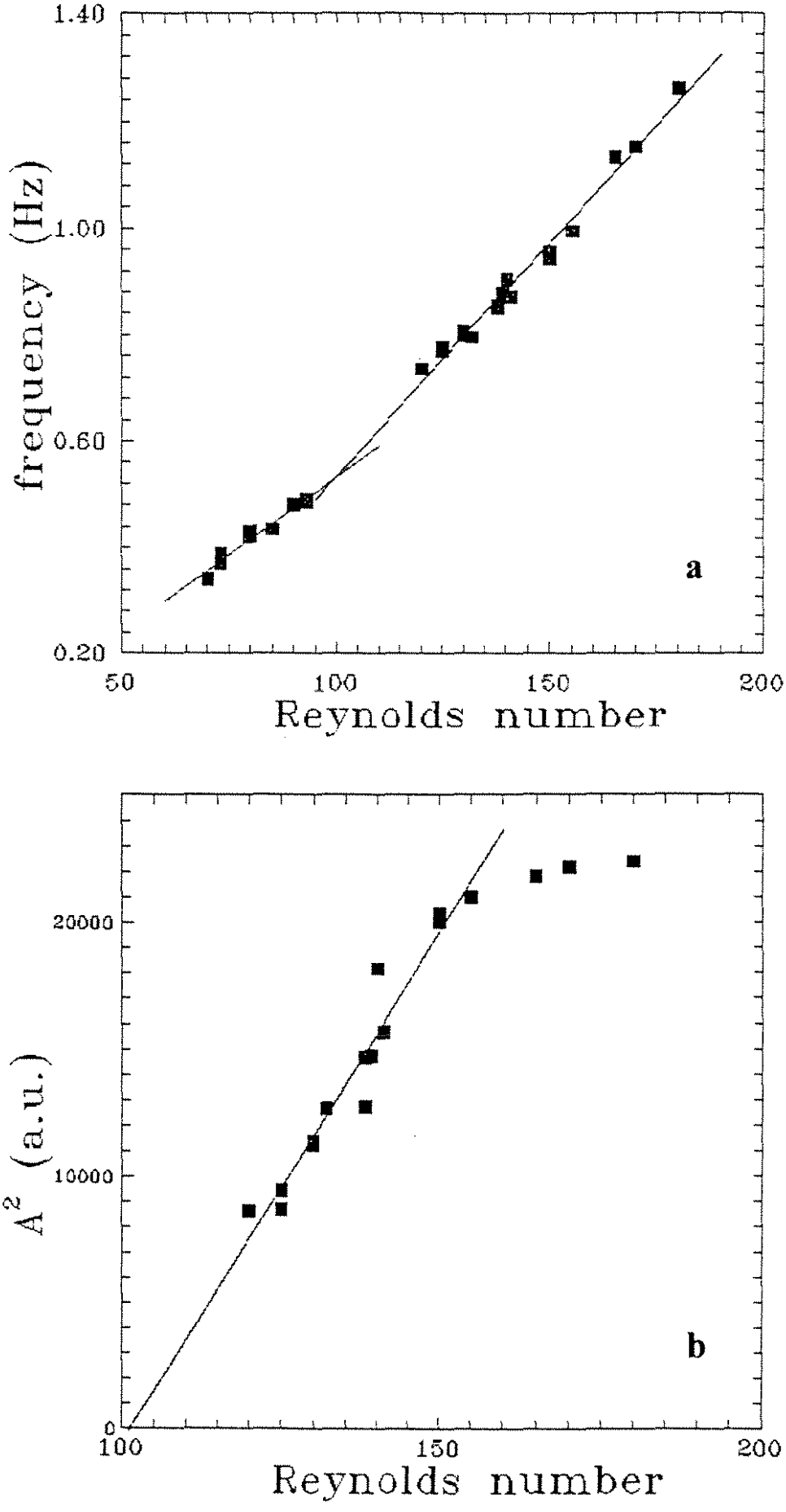

Figure 1: a) Variation of the wake frequency with the Reynolds number. b) Variation of the energy of the oscillations versus the Reynolds number. Note the saturation around R=160.

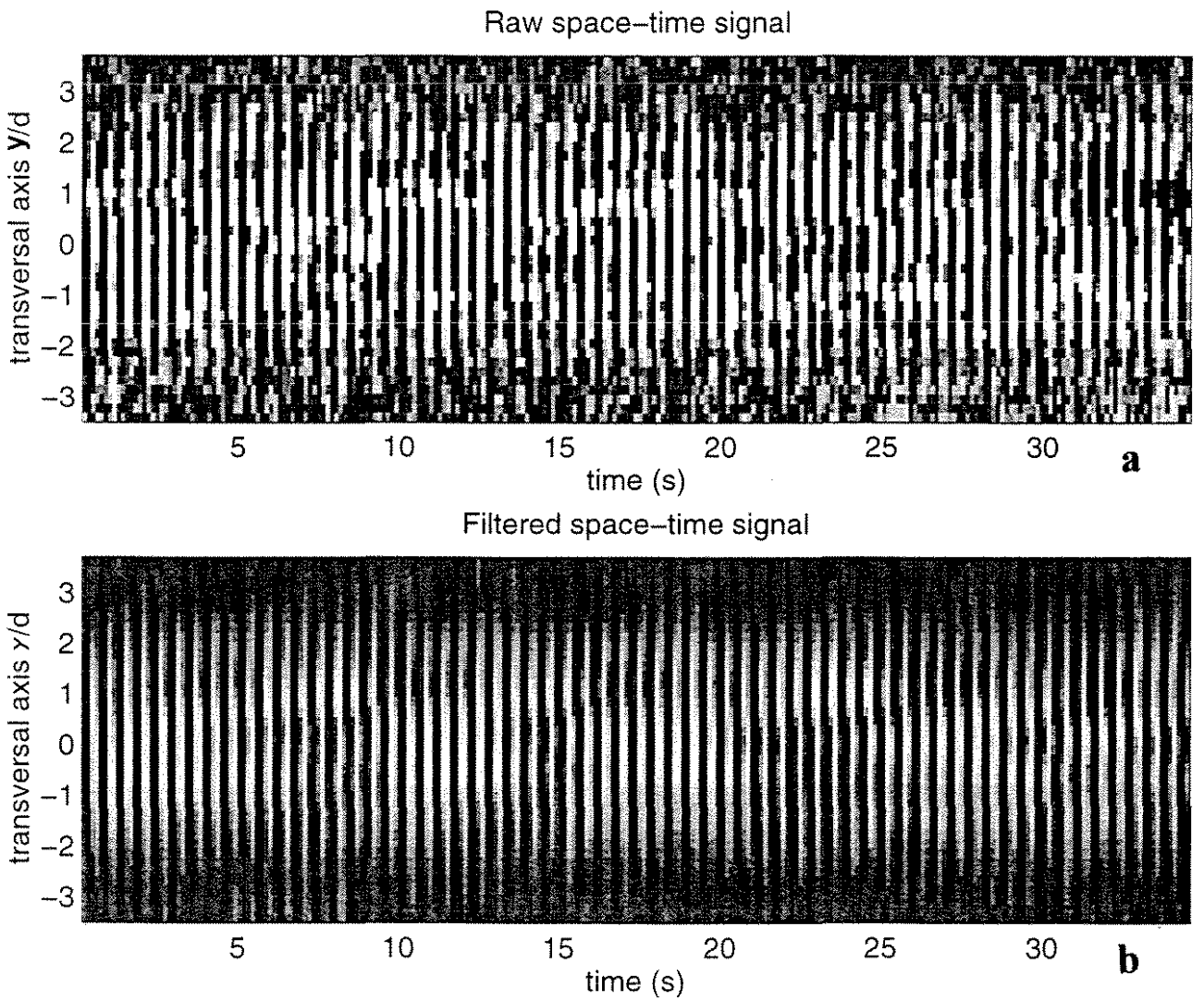

Figure 2: Space-time diagram of the transversal velocity component, a) raw data, b) filtered data (R=132, x/d=6).

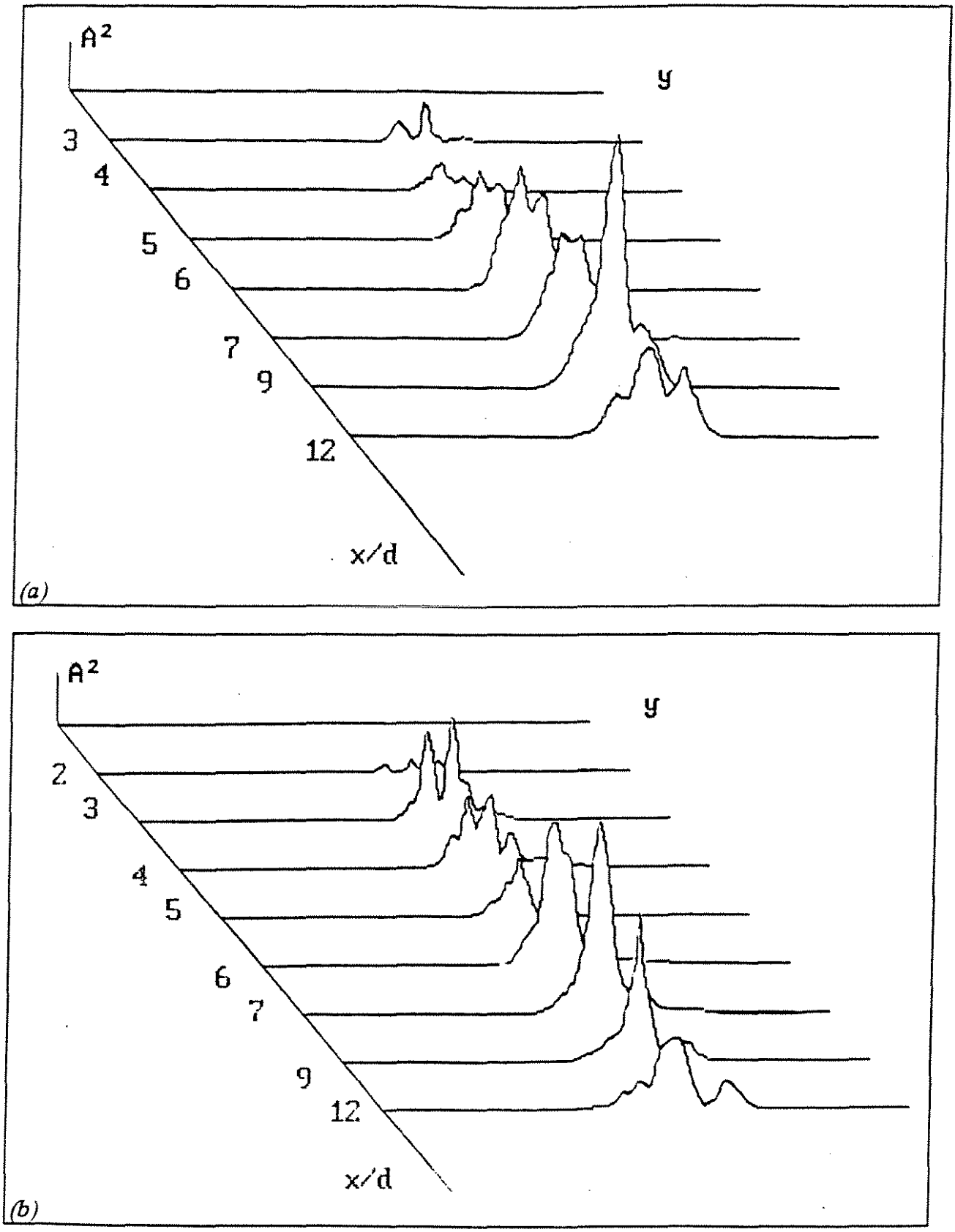

Figure 3: Three-dimensional representation of the spatial energy distribution of the transversal velocity oscillations. a)R=122, b) R= 142

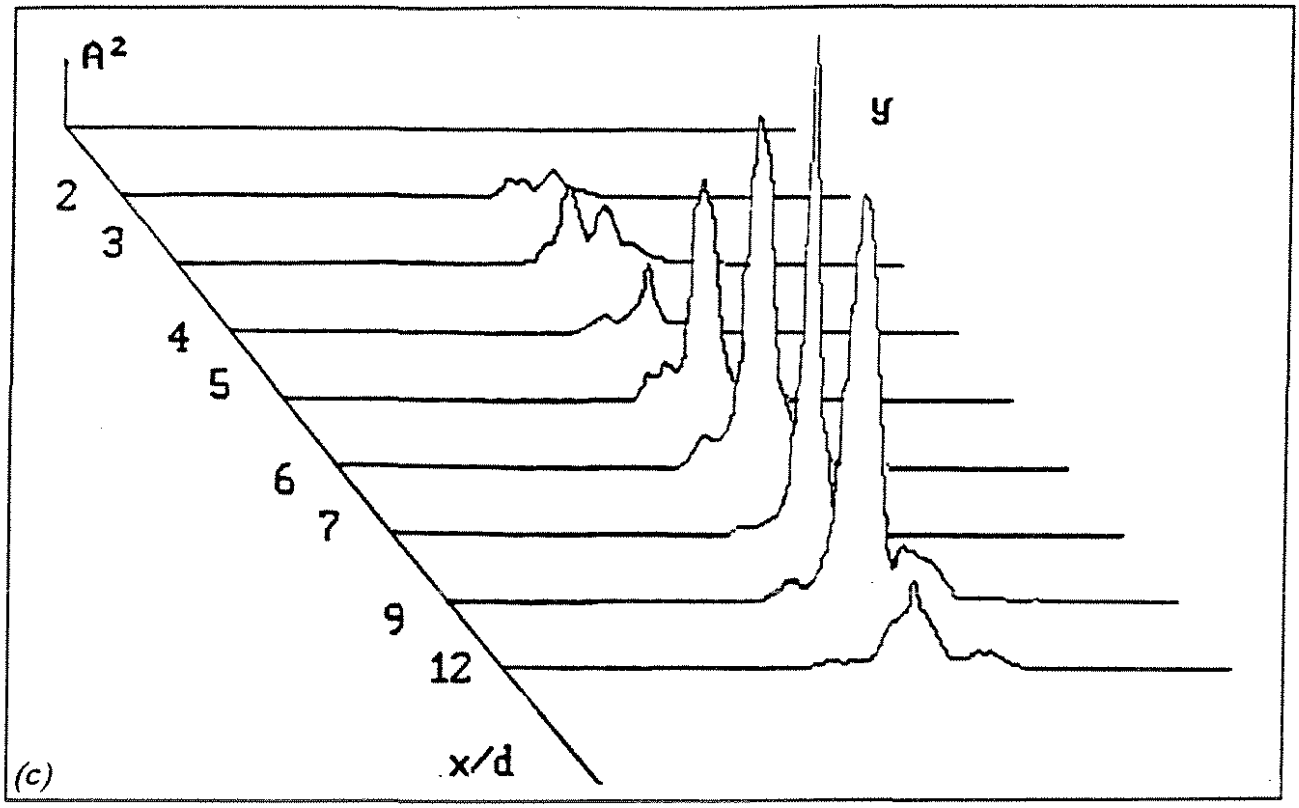

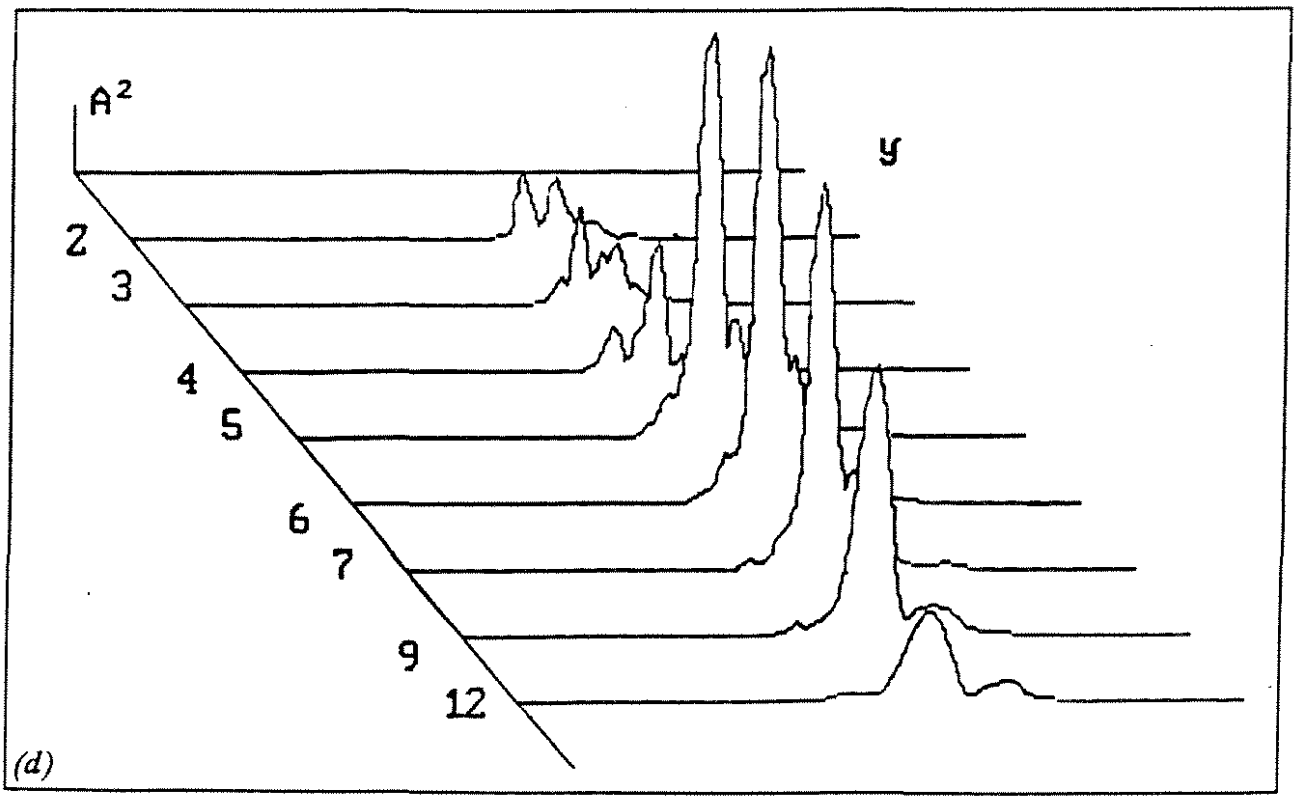

Figure 3: Three-dimensional representation of the spatial energy distribution of the transversal velocity oscillations. c)R= 170, d)R=185

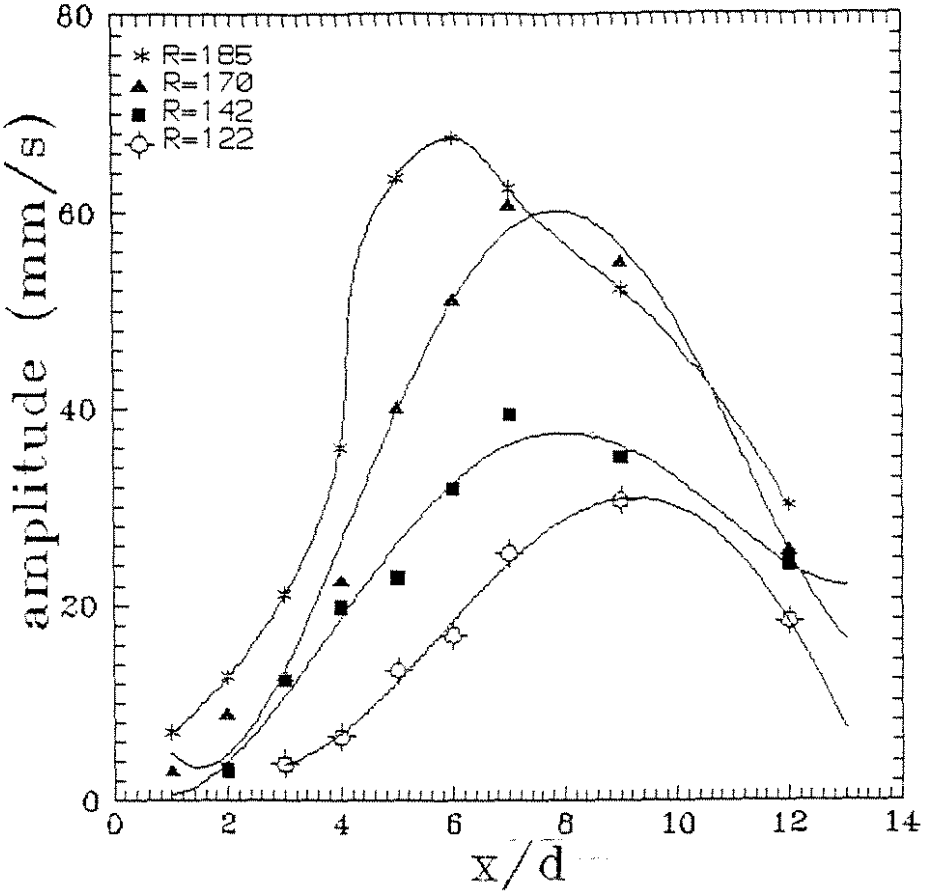

Figure 4: Amplitude of the transversal velocity oscillations downstream the cylinder (y/d=0) versus x/d for different Reynolds numbers.

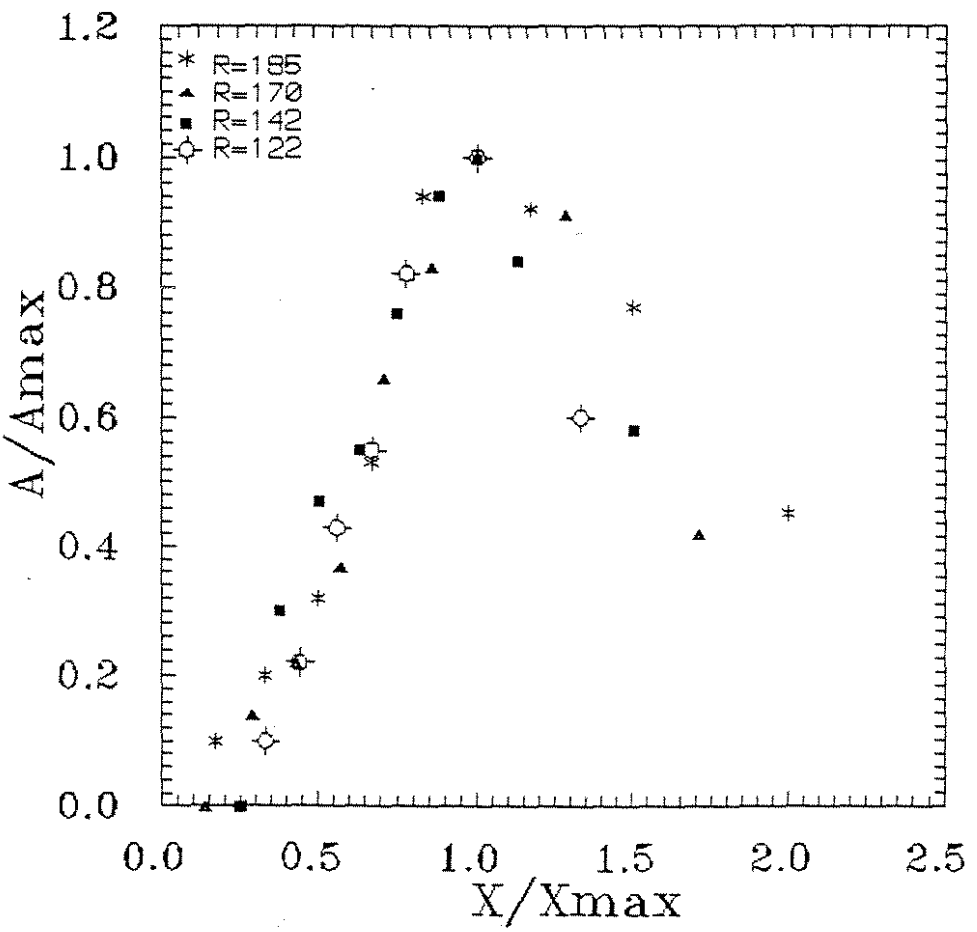

Figure 6: Renormalized amplitude of the transversal velocity oscillations downstream the cylinder (y/d=0) versus the renormalized longitudinal coordinate.

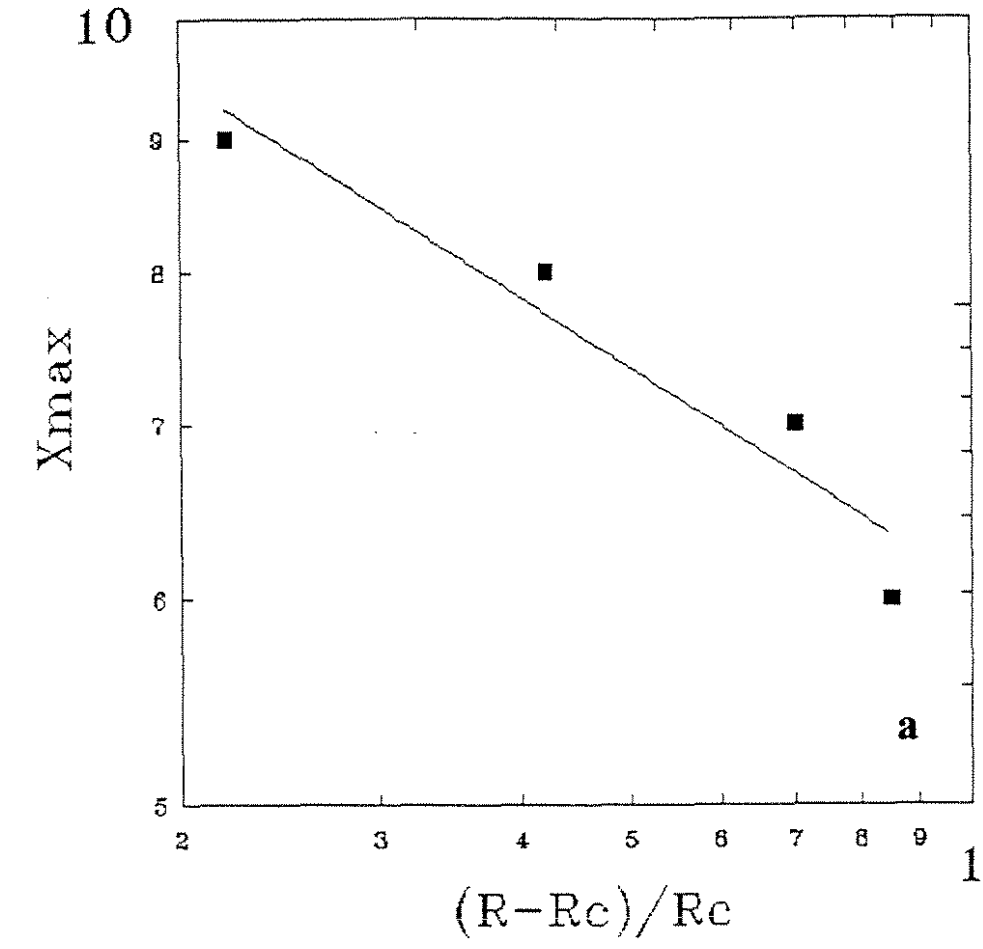

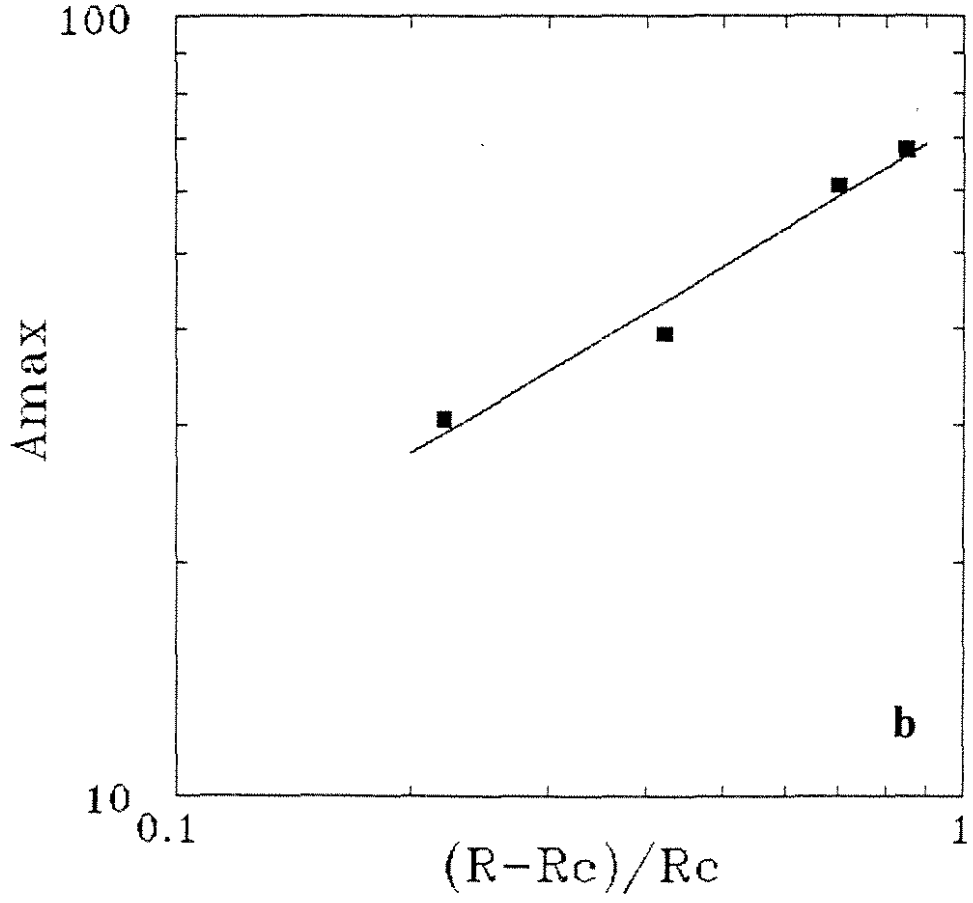

Figure 5: Log-Log plot of the position x_{max}(a) and of the amplitude A_{max} (b) of the maximum of the transversal velocity oscillations as a function of the Reynolds number.

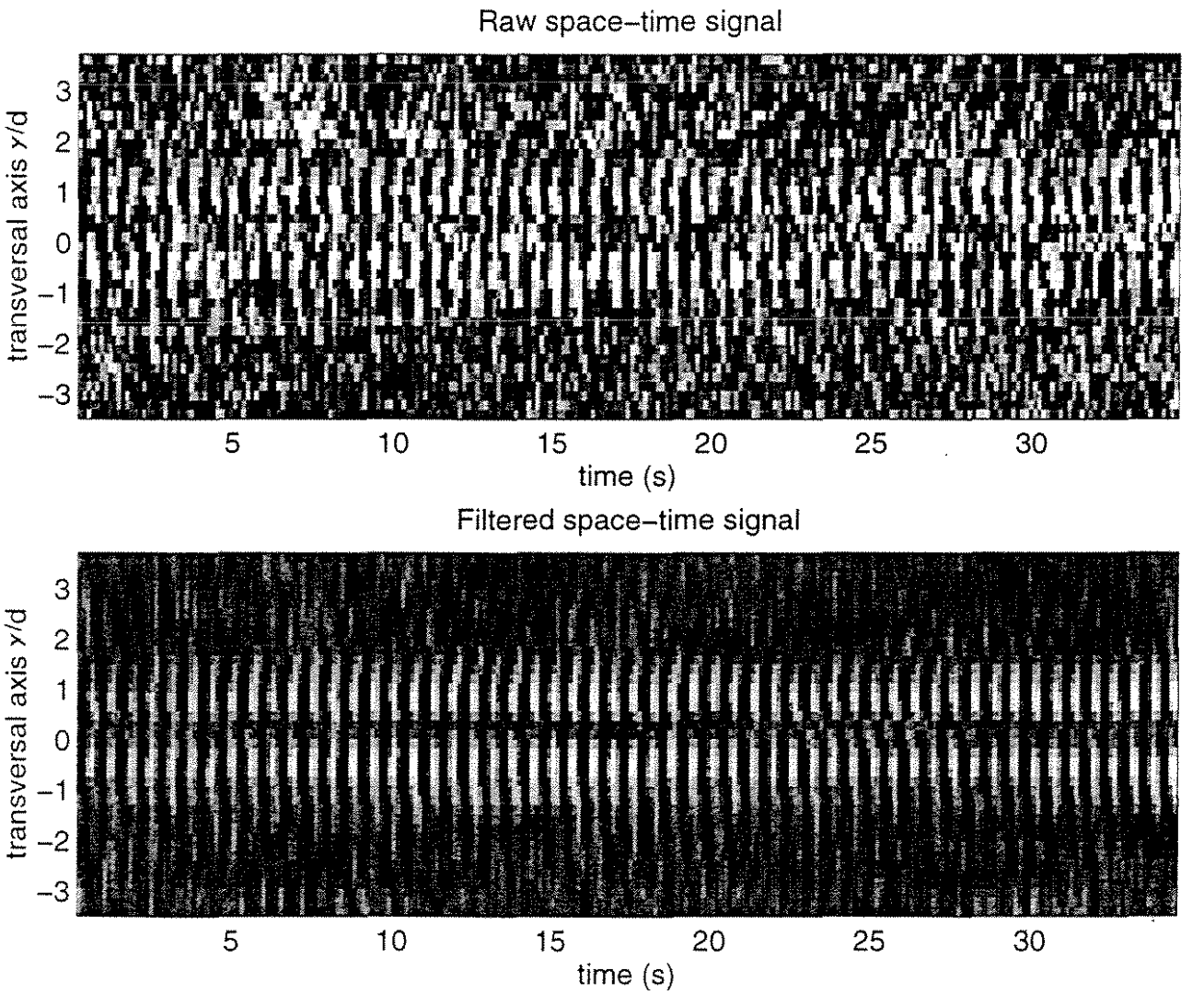

Figure 7: Spatio-temporal diagram of the transversal velocity component (R=120, x/d=2), gray scale coding of the velocity, a) raw data, b) filtered data. Note the sinuous mode of vortex shedding.

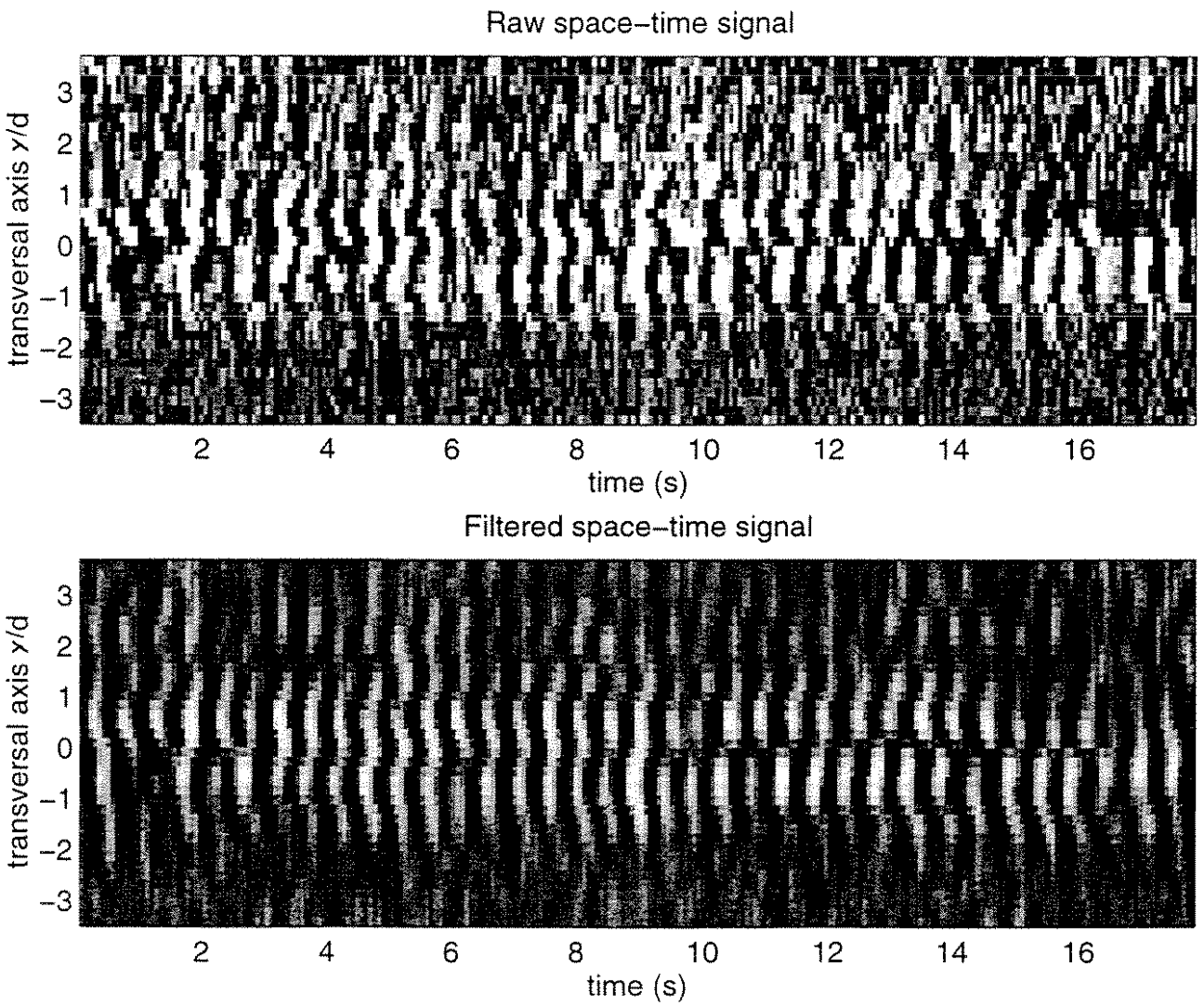

Figure 8: Space time diagram of the transversal velocity component (R=150, x/d=3), gray scale coding of the velocity, a) raw data, b) filtered data. Note the mixing of varicose and sinuous mode of vortex shedding.

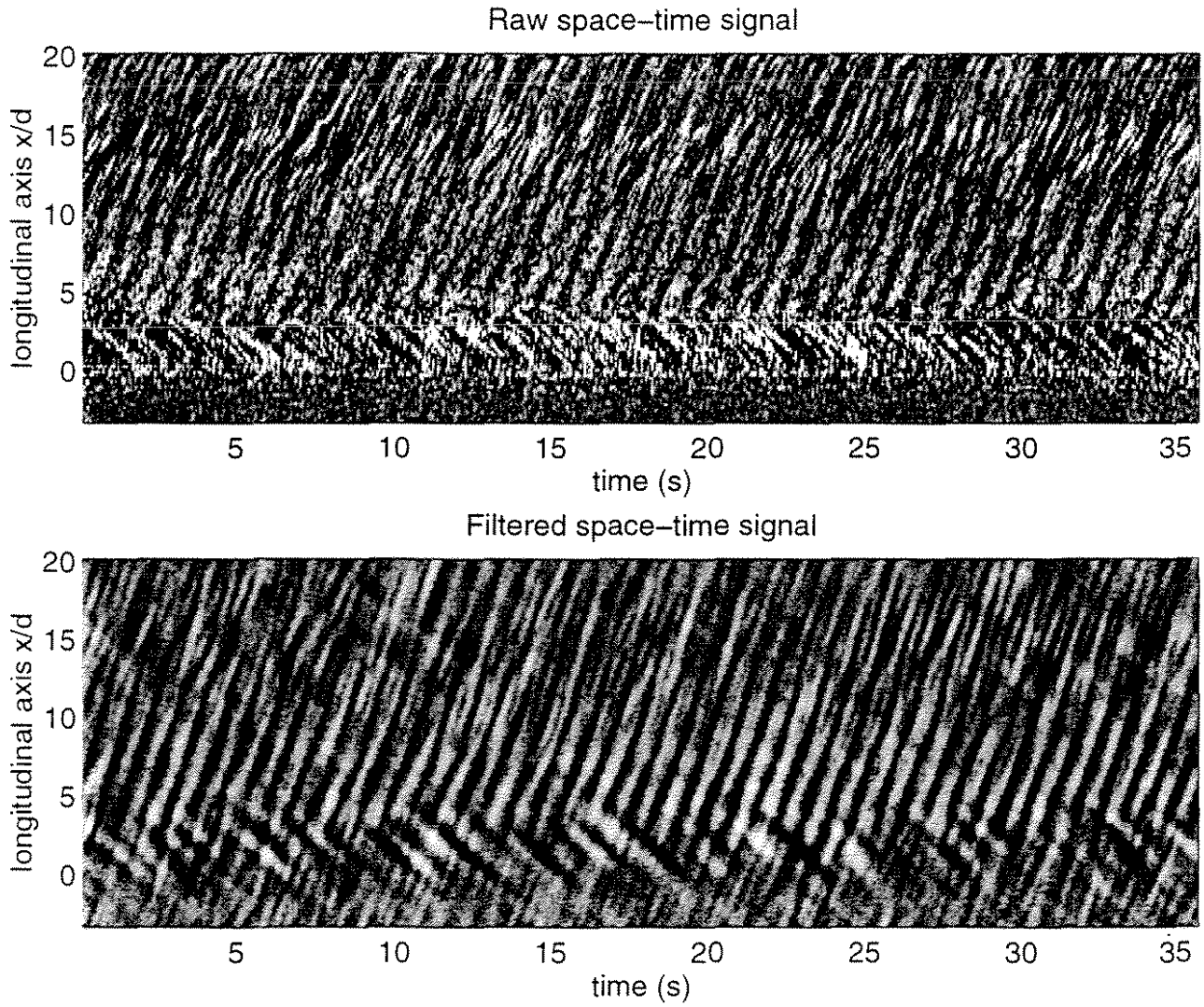

Figure 9: Spatio-temporal diagram of the longitudinal velocity component (R=132, y/d=0.5), gray scale coding of the velocity, a) raw data, b) filtered data.

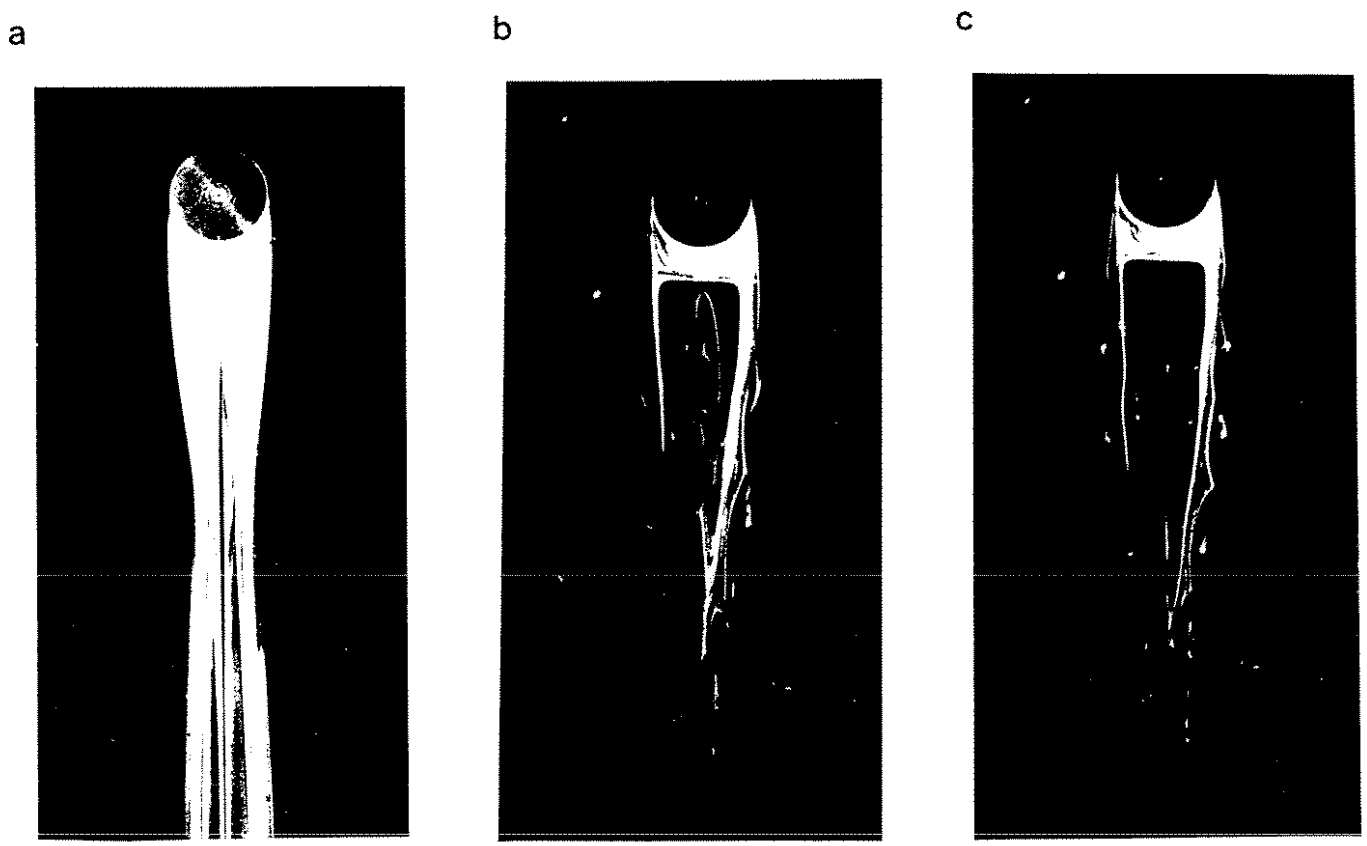

Figure 10: Snapshots of the near wake of a very small aspect ratio cylinder (l/d=0.5). a) R=300, b) R=450, c) R=500, d) R=750, e) R=800, f) R=900.